Flame Synthesis of Nanoparticles

By *Hendrik K. Kammler*, *Lutz Mädler*, and *Sotiris E. Pratsinis**

An overview of recent advances in the synthesis of nanoparticles by flame aerosol processes is given. In flame processes with gaseous precursors emphasis is placed on reactant mixing and composition, additives, and external electric fields for control of product characteristics. Thermophoretic sampling can monitor the formation and growth of nanoparticles, while the corresponding temperature history can be obtained by non-intrusive Fourier transform infrared spectroscopy. Furthermore, synthesis of composite nanoparticles for various applications is addressed such as in reinforcement or catalysis as well as for scale-up from 1 to 700 g/h of silica-carbon nanostructured particles. In flame processes with liquid precursors using the so-called flame spray pyrolysis (FSP), emphasis is placed on reactant and fuel composition. The FSP processes are quite attractive as they can employ a wide array of precursors, so a broad spectrum of new nanosized powders can be synthesized. Computational fluid dynamics (CFD) in combination with gas-phase particle formation models offer unique possibilities for improvement and possible new designs for flame reactors.

1 Introduction

Flame processes are by far the most widely used ones for the manufacture of commercial quantities of nanoparticles. The most important products today are carbon blacks made by Cabot, Columbia, Degussa-Hüls, etc., fumed silica (Cabot, Degussa-Hüls), pigmentary titania (DuPont, Ishihara, Millenium, Kerr-McGee) and optical fibers (Corning, Heraeus, Lucent, Sumitomo). The annual production volume of the flame industry is several million metric tons and typical production rates are of the order of 100 metric tons per day. The success and widespread application of this technology is based on its apparent simplicity of a one-step process and "no-moving parts" machinery. At the same time, this is a complex process as all product particle characteristics are determined within a few milliseconds and can be influenced by many process variables. Consequently, it is not surprising to find a large number of early patents claiming all sorts of tricks and gadgets to control product characteristics or to facilitate the operation of flame reactors [1]. As a result, a scientific understanding of flame synthesis of particles remains a major challenge even though a variety of scientific communities have studied it closely.

For example, in production of carbon blacks, pigments and fumed silica the focus is on understanding either how product particle size or crystallinity can be controlled within, say, 10 % of specifications, or how agglomerate formation can be suppressed to avoid expensive grinding processes. Agglomerates of large nanoparticles (300 nm) can be advantageous in the manufacture of optical fiber preforms by external processes where water or HCl has to be removed away from the preform prior to consolidation. Likewise, agglomerates of small nanoparticles (10 nm) are attractive in catalyst manufacture where the open structure allows for easy access to and from the particle surface by reactants and products. In contrast, there is a lot of interest in soot formation and suppression from an environmental science and engineering standpoint, and by utilities and automotive (especially diesel) manufacturers as well as in carbon film deposition processes.

During flame synthesis of particles, halide (or alkoxide) vapors are oxidized during the manufacture of ceramic oxides while fuel droplets are sprayed during the production of carbon blacks. This technology was developed by valiant evolutionary research, to the current rates of production of the order of 10 t/h. Recent advances in combustion and aerosol research have brought a new understanding of this technology and will be briefly summarized here. More specifically, it will be shown how reactant mixing, additives, or electric fields are used to control primary particle size and extent of agglomeration when gaseous precursors are used [2]. The use of non-intrusive temperature measurement techniques [3] combined with size independent thermophoretic sampling allows a unique view of the evolution of particle growth from single spherical to agglomerated nanoparticles [4]. These data can be used to develop models describing the evolution of particle growth [5] without adjustable parameters thus revealing the dominant physicochemical phenomena. Reactor design for flame synthesis of nanoparticles is now facilitated by interfacing these particle models with computational fluid dynamics (CFD) and particle dynamics [6,7]. Most importantly, CFD can be used to rank reactor designs for synthesis of particles with closely controlled characteristics [8].

In these reactors multicomponent particles can be made from gaseous precursors [9–11]. Using the above tools silica-carbon particles that can be used as fillers in the so-called "green tires" [12] can be made with closely controlled composition by controlling reactant composition or the electric field across the flame [13–15]. The scaling up of these reactors, making particles with controlled composition and morphology is investigated at production rates up to 700 g/h [16,17]. Multicomponent particles from these flames give rise to new products such as V_2O_5-TiO_2 catalysts with high selectivity at low temperatures [18].

Spray flame technology further broadens the options for synthesis of functional nanoparticles, as there are many liquid

[*] Dipl.-Ing. H. K. Kammler, Dr.-Ing. L. Mädler, Prof. Dr. S. E. Pratsinis (author to whom correspondence should be addressed), Institute of Process Engineering, ETH Zürich, Sonneggstrasse 3, CH-8092 Zürich, Switzerland.

  0930-7516/01/0606-0583 $ 17.50+.50/0

precursors available to make particles of complex composition [19]. Recently, flame spray pyrolysis (FSP) has been systematically investigated so as to make particles with closely controlled characteristics [20]. In these systems there are two distinct process regimes for particle synthesis depending on the competition between reaction and mass transfer. Furthermore, utilizing the framework of fuel spray combustion, models relating product characteristics to process variables are introduced, giving FSP a firm scientific basis for the synthesis of nanoparticles. This is particularly important, as FSP has not yet been utilized as widely by major industries as flame technology from gaseous precursors.

2 Nanoparticles by Combustion of Gases

Nanoparticles are made from gases by the so-called gas-to-particle conversion in flame reactors, hot-wall or furnace reactors, vapor-phase evaporation-condensation processes, plasma furnace reactors, laser and sputtering reactors, to name a few [2, 21–25]. The advantages of the gas phase processes are the production of particles of high purity composed of nonporous primary particles with small sizes, and relatively narrow size distribution. Disadvantages include difficulties in producing unagglomerated particles and multicomponent materials. Flame reactors are used in the industrial production of pigments (TiO_2) and reinforcing agents (carbon black and SiO_2) [1]. For example, the white pigment market has a world wide annual volume of about 3 Mio. t [26,27]. Half of it is made by flame technology, the so-called "chloride" process. In the USA and other developed countries most of the TiO_2 is used for paints (almost 50 %), in paper (25 %) and in the fabrication of plastics (20 %). The last 5 % is used as a pigment (inks, floor coverings, elastomers, roof granules, fibers, fabrics, sealants, foods, to name a few applications) and also has non-pigmentary uses (ceramics, welding rods, catalyst support, etc.) and other applications in specialty products [26]. Rutile TiO_2 particles are preferred in coatings and paints as they contribute a unique light scattering performance. For this, particles with a narrow size distribution around 200 nm and coated with a layer of SiO_2 are desirable [26].

Silica is used to control thickening, thixotropy, and reinforcement [28], as well as a stabilizer for suspensions, free flowing, or as a chemical mechanical polishing (CMP) agent [29]. Carbon blacks, however, are the most important fillers in rubber industries. Special properties like UV protection, electrical conductance, range of darkness, opacity and reinforcement can be achieved by adding carbon black particles to elastomers, plastics and paints [30].

2.1 Control of Flame Aerosol Reactors

A typical flame aerosol reactor set-up consists of a precursor unit (bubbler or evaporator), a burner accompanied by a gas delivery system and a filter unit to collect the product particles. Various flame configurations are used for the manufacture of nanoparticles, such as premixed and diffusion flames run in co-flow, or counterflow. In the diffusion flame configuration the fuel and the oxidizer diffuse into each other determining flame reaction and particle formation, while in premixed flames the precursor and the combustible gases are mixed before they enter the reaction zone (flame). A typical oxide particle producing premixed flame is shown in Fig. 1.

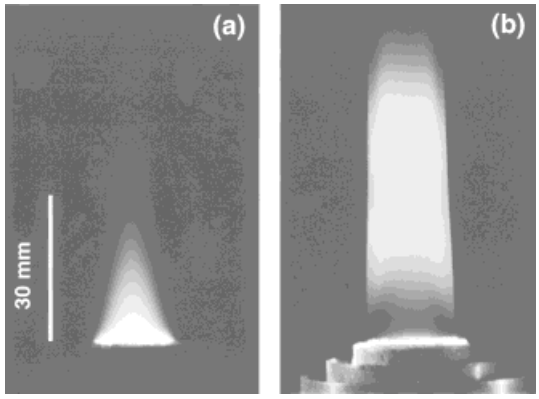

Figure 1. Premixed hexamethyldisiloxane (HMDSO)/methane/oxygen flat flame: (a) in the absence and (b) in the presence of a laser sheet.

In this oxygen-rich hexamethyldisiloxane (HMDSO)/methane/oxygen flame, the luminescence of the flame, Fig. 1a, is quite different to the trail of particle formation and growth as visualized with a laser sheet, Fig. 1b.

Depending on the gas flow rates and burner geometry, flames are either laminar or turbulent. In industry turbulent co-flow reactors are usually used, since large quantities of particles are desired. In academia, laminar flames are preferred as experiments are easier to describe with models in the laminar flow regime than in the turbulent one. Nevertheless, understanding of particle formation in turbulent flames is essential for optimal industrial aerosol reactor design.

2.1.1. Effect of Reactant Mixing

Flame temperature and particle residence time have been shown to be the most important parameters determining the characteristics of the product powder [2,21]. In flame aerosol reactors the flame temperature field is influenced mostly by the initial reactants and their mixing, and also by the burner geometry. Typical fuels are hydrogen, methane, or ethylene while oxidants are usually air or oxygen. Sometimes these gases are diluted with inert gases such as argon, helium, or nitrogen.

Reactant mixing, Fig. 2, can affect the product particle size by one order of magnitude [31]. Titania particles produced in a double (inverted) diffusion flame (primary particle diameter ~ 10 nm) (Flame A) were up to 10 times smaller than particles produced in a single (classic) diffusion flame (Flame D), where even non-agglomerated particles of a diameter of about

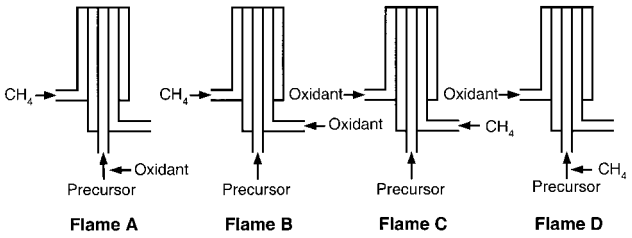

Figure 2. Reactant mixing configurations for a double or inverted (Flame A and B) and single or classic (Flame C and D) diffusion flame reactor [2].

100 nm were made [31] as proven by small angle X-ray scattering [32]. The inverted diffusion flame always produced finer particles (SiO_2, SnO_2, TiO_2, Al_2O_3) than the classic diffusion flame due to lower temperatures in the former flames [6,31,33,34].

Operating a diffusion flame reactor with oxygen instead of air, Zhu and Pratsinis [33] increased the size of silica product particles by about 5 times in a single $SiCl_4$/methane diffusion flame (Flame C). In inverted diffusion flames (Flame B) this difference was less pronounced, as only 50% larger particles were formed with oxygen when compared to air as the oxidant. Using oxygen leads to faster fuel consumption, and therefore to higher flame temperatures and to shorter flames, thus, the precursor oxidation as well as growth and sintering is enhanced. In a similar set-up, Briesen et al. [35] found a similar increase of the primary product particle size investigating different silica precursors ($SiCl_4$, hexamethyldisiloxane (HMDSO), and octamethylcyclotetrasiloxane (OMCTS)), when they replaced air by oxygen.

For SnO_2 particles from $SnCl_4$ the choice of oxidant (air or oxygen) did not affect the average primary particle size, even though the primary particle size could be closely controlled by the oxidant flow rate as for SiO_2 [33]. For the same flow rates, however, only the flame configuration and therefore reactant mixing affected the SnO_2 product particles [33]. It could be seen that particles produced in an inverted diffusion flame (Flame B) were 1.8–2.4 times smaller than the ones made in a single diffusion flame (Flame C). For Al_2O_3 particles made from aluminium-tri-sec-butoxide Johannessen et al. [6] observed particles with 1.2–1.4 times larger specific surface areas in the inverted diffusion flame (Flame B) set-up compared to particles made in a single diffusion flame (Flame C).

For titania the oxidant did not affect the size of the average primary particle in inverted diffusion flames (Flame A, B), while significantly larger TiO_2 particles (2–3 times) were formed in single diffusion flames (Flame C) substituting air by oxygen [34]. In a classic diffusion flame (Flame C) the rutile content was progressively retarded from 13.2 to < 0.1 wt% by increasing the oxygen concentration of the oxidant from 21 % (air) to 100 % (pure oxygen). However, in an inverted diffusion flame (Flame B) the rutile content remained constant (about 8 wt%) for all the oxidant compositions investigated. At these conditions an increasing number of perfectly spherical unagglomerated particles (200–300 nm) were made by increasing the oxygen concentration of the classic diffusion flame (Flame C).

Wegner and Pratsinis [8] showed that reactor geometry could also significantly change product powder characteristics. Using the same gas and precursor flow rates as Briesen et al. [35], they produced primary silica particles which were 4 times smaller using HMDSO in a reactor with a diameter about a quarter of the one used by Briesen et al. [35]. The enhanced mixing of the gases in the smaller reactor leads to a steeper temperature gradient as confirmed by CFD calculations. Furthermore, the burner outlet velocities are significantly higher compared to Briesen et al. [35], which reduces the residence times of the particles in the hot flame zone and consequently there is less time for growth and sintering.

2.1.2. Effect of Precursor

Zachariah and Semerjian [36] and Ehrman et al. [37] investigated different silica precursors and did not observe significant effects on SiO_2 particles. However, the choice of precursor becomes important when a considerable amount of heat is provided by the combustion of the precursor itself [35]. This becomes more pronounced for higher precursor concentrations [16,17]. Silica particles made from organosilicon compounds had significantly lower specific surface area than those produced from $SiCl_4$ [35] for all investigated oxidant flow rates in diffusion and premixed aerosol flame reactors. In premixed flames Briesen et al. [35] correlated the specific surface area of the product with the adiabatic flame temperature, which is determined by the choice of precursor.

Besides altering the flame structure, the amount of precursor introduced into the flame determines the collision frequency of the particles during the growth process. Pratsinis et al. [31] found that the specific surface area of the titania particles was halved by increasing the inlet $TiCl_4$ concentration by a factor of 10 for inverted diffusion flames (Flame B). Similarly, the specific surface area was decreased by 1.4–1.6 times in single diffusion flames (Flame C) consistent with Formenti et al. [38] and Ulrich et al. [39] making SiO_2 from $SiCl_4$. However, Ulrich and Riehl [40] observed that the flame temperature is more important than SiO_2 concentration for the particle specific surface area. For silica production in pure HMDSO/oxygen double diffusion flames Kammler and Pratsinis [16] found that the specific surface area of silica product powders decreased from 175 to 22 m^2/g quadrupling the HMDSO concentration. As HMDSO was the only fuel in these experiments, increasing the HMDSO concentration increased the energy content of the flame, thus, the flame temperature and SiO_2 concentration were increased. At higher flame temperatures the growth and sintering rates are enhanced and increasing the SiO_2 concentration increased the collision frequency of the particles. Additionally, the flame height increased as more fuel was introduced, increasing the residence time of the particles in the flame, and therefore prolonging the time for growth and sintering, resulting in the observed low product specific surface areas.

2.1.3. Effect of Additives

Additives can be used to control the primary particle size or crystallinity and the extent of agglomeration when the purity of the product powder is not a primary concern [2]. For example, small amounts of $AlCl_3$ are injected to promote the formation of rutile titania and to moderate aggregation in its manufacture from the chloride process [26]. Vemury et al. [10] studied the effect of additives on phase composition, morphology and size of titania product particles in laminar diffusion flames doping the $TiCl_4$ stream with various amounts of $SiCl_4$, $SnCl_4$, and $AlCl_3$, respectively. They found that doping the titania with silica inhibits the titania phase transformation from anatase to rutile, and decreases the primary particle size, thus, increases the specific surface area. In the flame reactor significantly larger amounts of silica had to be added to completely inhibit the phase transformation from anatase to rutile compared to particles made in electrically heated hot-wall reactors [41] as the temperature and residence times of the particles are less homogeneous in flame aerosol reactors. Furthermore, the addition of $SnCl_4$, and $AlCl_3$ promoted the anatase to rutile phase transformation and increased the average primary particle diameter. For example, the addition of 20 mol% $AlCl_3$ reduced the specific surface area of the product powder from 54 to 35 m^2/g. However, more dopant had to be added to the flame reactor in order to achieve identical product powder crystallinity compared with powders made in the hot wall reactor [42]. In silica synthesis Fotou et al. [43] observed that adding ferrocene to $SiCl_4$ in methane/air diffusion flames led to an increase in the specific surface area of the silica product powder of up to 150 %. Additives are widely used in the carbon black industry to control the morphology of the product even though their exact mechanism is not well understood.

2.1.4. Effect of External Electric Fields

For precise control of the product powder characteristics, external electric fields have been shown to be quite effective and are intriguing as they can be readily implemented into the reactor set-up. The newly formed particles are charged in the electric field either by ion or electron attachment, so the coagulation rate of the particles is reduced, as unipolarly charged particles repel each other. Charged particles are also attracted towards electrodes, thus lowering the local particle concentration and therefore the collision rate. The flame structure, height, and temperature are also altered by the electric field, which can significantly influence the particle residence time at high temperatures and therefore affect particle growth and sintering. It was shown, that external electric fields can reduce the average particle size by up to a factor of two as determined by nitrogen adsorption [44–47]. Fig. 3 shows the narrow control of the specific surface area of titania product particles by the electric field strength between two electrodes across the flame flow.

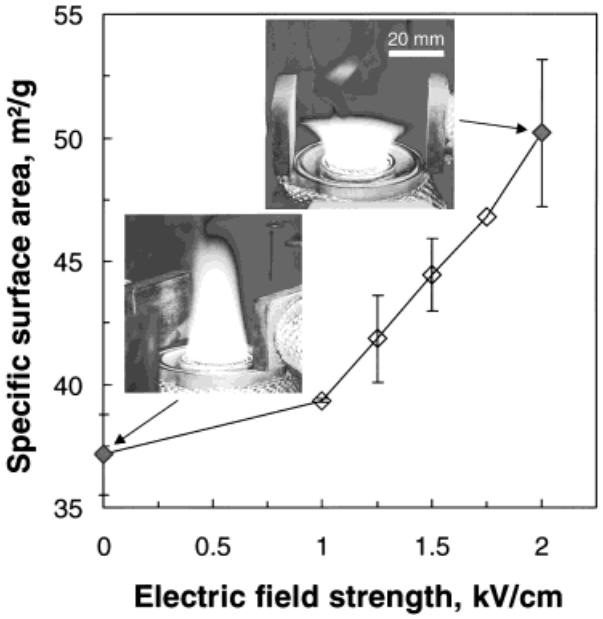

Figure 3. Specific surface area of the TiO_2 product powder made by titanium tetraisopropoxide (TTIP) oxidation in a premixed methane/oxygen flat flame as a function of the applied electric field strength.

Increasing the electric field strength flattened the flame as shown by the inserts in Fig. 3. Recently, Kammler and Pratsinis [14] demonstrated that external electric fields can also precisely control the specific surface area of the product powders at SiO_2 production rates up to 87 g/h. They further confirmed that the positioning of electrodes near the decisive particle formation zone of the flame is necessary for successful operation of the electric fields [44].

In premixed honeycomb-stabilized flat flames Vemury et al. [46] made TiO_2 consisting of pure anatase (99.9 %), the electric field did not change the powders crystallinity. Using non-stabilized premixed flames, however, they could control the rutile fraction from 82 to 65 % by increasing the electric field strength between two needle electrodes from 0 to 2.75 kV/cm [46]. In a diffusion burner set-up, they decreased the rutile content of TiO_2 powders steadily from 20 to 8 wt% using electric field strengths between 0 and 1.75 kV/cm, respectively [44]. In contrast to reactant mixing, electric fields are effective for precision control over a narrow range (up to a factor of 2) and as such can find applications as a control device or for synthesis of functional nanoparticles with highly sensitive properties with respect to particle characteristics.

2.1.5. Monitoring Particle Growth in Atmospheric Flames

The growth of particles is mostly determined by the flame temperature and particle residence time [21]. Therefore, it is of great importance to have accurate temperature profiles in flame aerosol reactors. In principle, conventional laser diagnostic methods are limited for application in particle laden flames, as interferences of the response signal with particulate matter may weaken signal intensity and increase

the complexity of signal evaluation. Recently, however, laser-induced fluorescence (LIF), that has been used in gas phase combustion [48], was successfully used in dilute particle laden low pressure flames to measure flame temperature and to detect local concentrations of SiO [49,50], FeO [51], AlO and TiO [52].

Fourier transform infrared (FTIR) spectroscopy has been used to reliably determine flame temperatures in the presence of soot, silica and titania [3, 53–55] and even inside an electrically assisted flame [3]. FTIR relies on emission/transmission measurements to calculate the normalized radiance, which can be directly compared to a blackbody Planck function to determine the flame temperature [56]. Comparison of this technique with other flame diagnostics such as thermocouple injection methods or coherent anti-Stokes Raman spectroscopy (CARS) in an ethylene-air diffusion flame demonstrates the strength of this technique [53, 57,58].

Fig. 4 shows an axial flame temperature profile of a premixed HMDSO/methane/oxygen flat flame, converting 20 g/h HMDSO to nanosized SiO_2 particles.

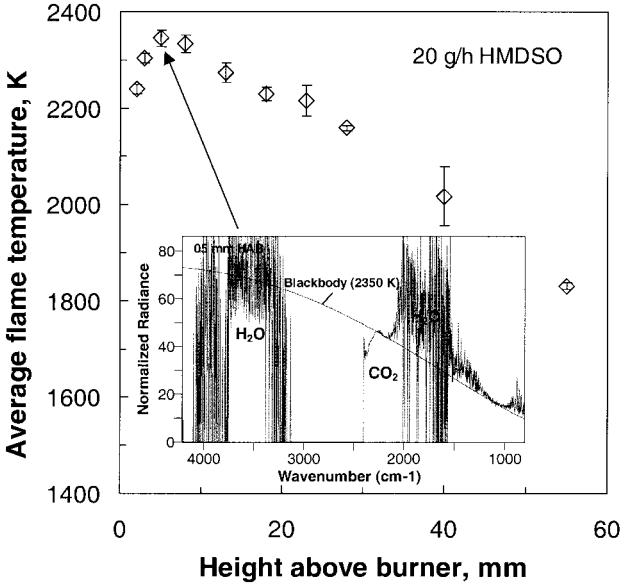

Figure 4. Axial temperature profile of a premixed HMDSO/methane/oxygen flat flame. In the lower part of the figure a typical comparison of the normalized radiance spectrum with the blackbody Planck function is shown, using a least squares fit at the wavenumber range of hot CO_2 (2200–2300 cm^{-1}). Species detectable at other wavenumber ranges are named.

The temperature rises quickly and decreases slowly with increasing distance, which is typical for premixed flames [59]. In Fig. 4 a typical evaluation scheme of the temperature at a flame height of 5 mm is included, in which the normalized radiance spectrum of the flame is compared to a blackbody Planck function of a certain temperature. This match is achieved by a least squares fit in the wavenumber range of hot CO_2 (2200–2300 cm^{-1}). H_2O is detected at 4000–3500, 1800–1200, and 800–600 cm^{-1} and the blackbody Planck function at the matched temperature fits these bands reasonably well.

Arabi-Katbi et al. [4] and Pratsinis et al. [5] monitored particle growth in premixed titanium tetraisopropoxide (TTIP)/methane/oxygen flat flames with thermophoretic sampling [60,61]. They measured axial flame temperature profiles for various particle concentrations by FTIR at exactly the same locations where the particle growth was monitored by a thermophoretic sampler. Fig. 5 shows the evolution of TiO_2 particle growth along the height above the premixed TTIP/methane/oxygen flame as obtained by thermophoretic sampling in our laboratories.

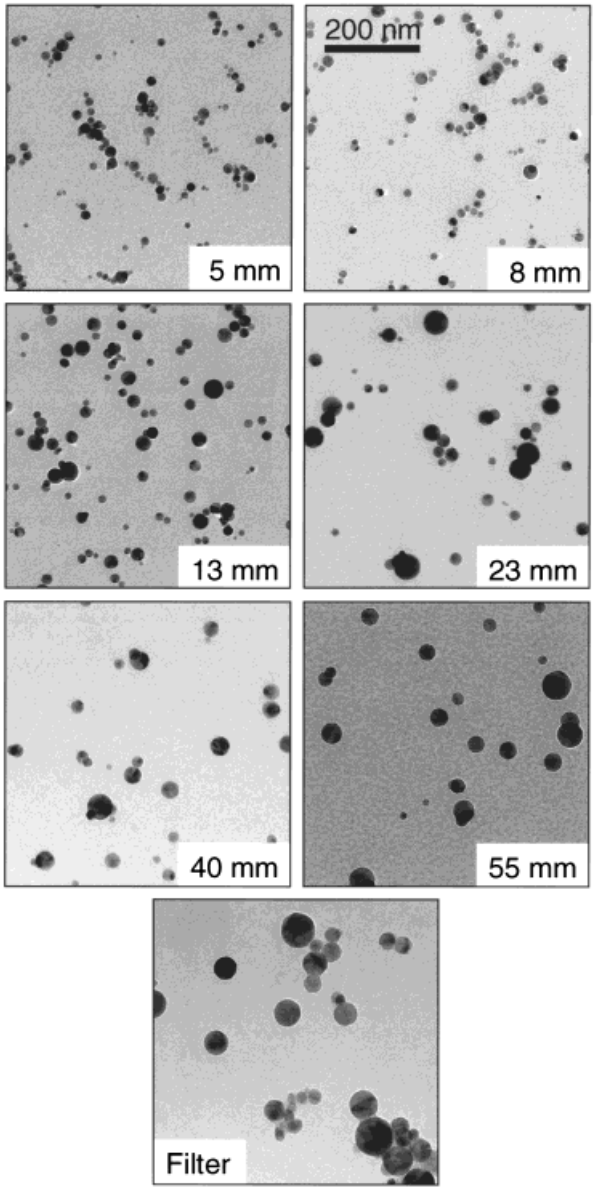

Figure 5. TEM pictures of TiO_2 particles at increasing heights above the burner as obtained by thermophoretic sampling in a premixed TTIP/methane/oxygen flat flame.

At low heights, small agglomerate formation was observed, while the particles are almost non-agglomerated and perfectly spherical at higher positions, before agglomeration sets in at even higher positions (close to the filter). The particles grow

rapidly close to the burner and the growth levels off further downstream, when the flame temperature is reduced. These data now can be compared with particle dynamics models as will be discussed in Section 4 of this paper.

Alternatively, in low pressure premixed flames Lindackers et al. [62–64] applied aerosol mass spectroscopy (AMS; a combination of a quadropole mass spectrometer with cross-beam ion source and a particle mass spectrometer [65,66]) to monitor the particle size evolution with increasing distance from the burner. Silica particle diameters [63], as well as those of alumina and tin oxide nanoparticles [62] increased from 3.0 to 7.6 nm, 4.7 to 8.4 nm, and 2.7 to 8.3 nm, respectively, increasing the distance between the burner and the sampling nozzle from 20 to 80 mm. The flame temperature profiles were calculated using the PREMIX code from Sandia National Laboratories [67] and are included in a particle growth model accounting for particle formation and growth by Brownian coagulation [63].

2.2 Multicomponent Particles

A mixture of precursors can be used to produce multicomponent particles, which can have special properties such as superconductivity [68], superparamagnetism [11], or increased catalytic activity [18], for example. The formation of multicomponent particles from gaseous precursors in counterflow diffusion flame reactors has been extensively investigated by Katz and co-workers [9, 69–72] making TiO_2/SiO_2, Al_2O_3/TiO_2, SiO_2/GeO_2, V_2O_5/TiO_2, V_2O_5/Al_2O_3, and VPO.

Zachariah et al. [11] studied the synthesis of mixed iron-silica particles and found that 5–19 nm Fe_2O_3 particles embedded in much larger SiO_2 particles exhibited superparamagnetic behavior. In premixed aerosol flame reactors Ehrman et al. [73] investigated binary SiO_2/TiO_2 and SiO_2/Fe_2O_3 nanoparticle formation by varying the Ti or Fe to Si mole ratios. Phase segregation was observed to varying degrees in qualitative agreement with segregation expected from binary phase diagrams for the bulk systems. Differences between the SiO_2/TiO_2 and SiO_2/Fe_2O_3 systems were explained by considering the variation in the thermodynamically stable liquid-phase solubility and differences in the ability of iron and titanium ions to substitute for silicon ions in the network structure.

2.2.1. Vanadia Coated Titania Nanoparticles for Selective Catalytic Reduction of NO

In various applications segregated phases may be advantageous. For example maximum activity and selectivity of vanadia coated titania catalysts is achieved when the vanadium oxide is present as an amorphous mono-layer at the surface of the titania particles [74]. Vanadia coated titania is a well known catalyst e.g. for the selective oxidation of o-xylene to phthalic anhydride [27] or for selective catalytic reduction (SCR) of NO by NH_3 [75]. This catalyst is typically prepared in liquid phase processes. Nevertheless, Katz and co-workers [9, 71, 72] produced titania nanoparticles in a counterflow diffusion flame with 14, 25, and 50 wt% vanadia from $TiCl_4$ and $VOCl_3$, however, they did not report the activity of their product. Stark et al. [18] synthesized spherical titania particles coated homogeneously with amorphous vanadia in a co-flow diffusion flame from titanium tetraisopropoxide and vanadium oxotriisopropoxide. Flame generated titania formed small spheres with diameters of 10 to 50 nm. Using high-resolution transmission electron microscopy (HRTEM) no interstitial solution of vanadium was found inside the titania lattice. Lattice fringes were discernible up to the surface of the particles corroborating their monocrystalline structure [18]. X-ray photoelectron spectroscopy analysis indicated that the vanadia was dispersed on the surface of the titania particles. The vanadia content (0–10 wt%) did not influence the specific surface area of the product powder, while the specific surface area was increased significantly from 23 to 120 m^2/g, by increasing the oxygen flow rate from 2 to 10 L/min. Adding more oxygen to the flame accelerates the oxidation process as fuel-oxidant mixing is enhanced [8], thus, the flame height decreases and the excess oxygen cools the flame. This leads to smaller particles as sintering rates decrease with decreasing temperatures and particle residence times reduce due the faster gas flow rate and reduced flame height. These V_2O_5 coated TiO_2 catalyst particles were tested in the conversion of NO to N_2 at low temperatures in a continuous fixed flow reactor [76, 77] at a global space velocity of 24000/h [18].

In Fig. 6 the performance of a flame-made catalyst (diamonds) and a catalyst prepared by wet chemistry (circles) [78] are compared at different catalyst temperatures.

At a catalysis temperature of 480 K the NO is completely converted to N_2 by the flame-made catalyst, while at the same temperature only 92% of NO is converted to N_2 by the wet-

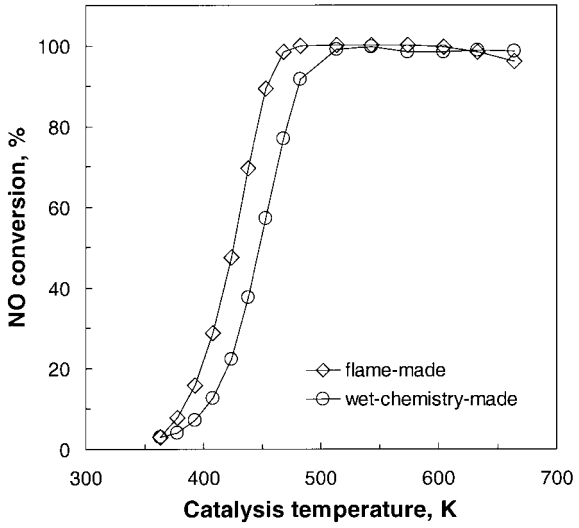

Figure 6. NO-conversion as a function of catalysis temperature for a flame-made (diamonds) and wet-chemistry-made (circles) vanadia coated titania catalyst (courtesy of W. J. Stark, ETHZ).

chemistry-made catalyst. One can clearly see that the flame-made catalyst can compete with state of the art catalysts, and it shows even slightly better performance even at lower process temperatures.

2.2.2. Silica-Carbon Composite Particles

The combination of carbon black and silica in composite particles [79] is more effective in reinforcing rubber compared to carbon black alone, providing the potential to make the so-called "green tires". The silanol groups on the silica surface together with an organosilane coupling agent are used to form a silica network in the rubber, which enhances the tire reinforcement as it decreases the rolling resistance by up to 24 % [80]. The wet traction and tread wear are similar to that of conventional tires [12], while decreasing the rolling resistance of car and truck tires significantly decreases fuel consumption (3–5 % and 6–8 %, respectively) [80]. The specific surface area of silica powders in green tires should be lower than 180 m^2/g [81] and the carbon ensures good dispersibility and static electricity dissipation [12,30].

Various SiO_2-C powder composites with a carbon content of up to 30 % were synthesized by Spicer et al. [15] from $SiCl_4$ and acetylene in a premixed flame. They found a significant increase in the carbon black yield (up to three times) by the presence of silica compared with a pure acetylene flame of the same equivalence ratio. The silica particles acted as seed nuclei for carbon surface growth, while the presence of chlorine reduced the flame temperature favoring enhanced carbon (soot) formation. Kammler and Pratsinis [16] made silica-carbon particles with carbon content up to 5 wt% in a ring shaped HMDSO/oxygen double diffusion flame at production rates up to 130 g/h. Soot formation (up to 2 wt%) during silica synthesis was also reported by Briesen et al. [13] producing 30 g/h of powder in electrically assisted flames as well as by Kammler and Pratsinis [14]. The latter could precisely control the product powder carbon content (0–1 wt%) with the electric field intensity.

2.3 Pilot-Scale Production of Nanoparticles

Scaling-up flame aerosol reactors used to involve tedious Edisonian research to make product powders with closely controlled characteristics, even though the flame aerosol process has been utilized in industry for more than 50 years [82]. However, large-scale production of new materials or special composite particles can comprise a similar evolution of steps. Therefore, fundamental research has to be conducted on pilot-scale reactors in order to establish a connection between small-scale laboratory units and their large-scale counterparts. Applying the principles of scale-up in reactor design is not as straightforward as one might wish. In many cases it is impossible to simultaneously satisfy scale-up constraints called for by different forms of similitude. Therefore, databases have to be created in order to evaluate the key parameters of these processes.

As an example, the continuous production of silica and silica-carbon nanostructured particles with controlled composition and morphology is presented, at production rates up to 700 g/h and up to 10 % solid fraction by mass, which is close to that of industrial processes. These particles were made in a turbulent single diffusion flame reactor, Fig. 7, using hydrogen and air as fuel and oxidizer, respectively.

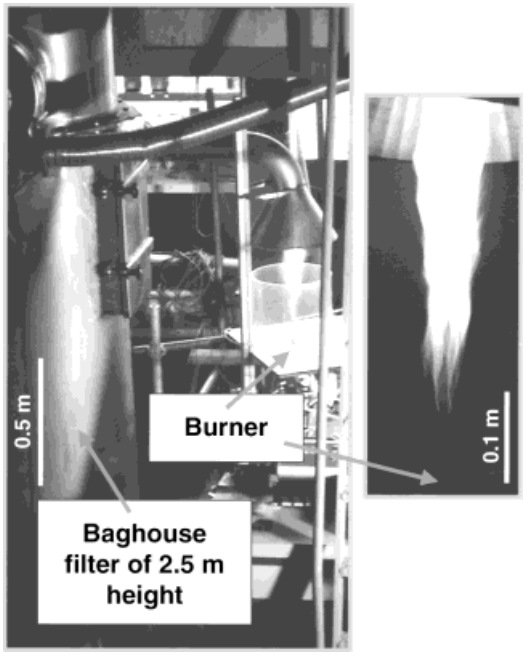

Figure 7. Photograph of a pilot-scale flame aerosol reactor, which can produce nanostructured silica-carbon powders at production rates up to 700 g/h.

On the left-hand side of Fig. 7 the baghouse filter can be seen, which allows continuous powder production as demonstrated by operating for 5 h at a production rate of 700 g/h [17]. In Fig. 7 the particle producing flame is shown with the collection pipe above the flame connected to the baghouse filter. On the right hand side, a typical silica particle producing flame is shown. The specific surface area of the product powders was controlled by reactant stream composition in the range of 75 to 250 m^2/g, corresponding to average primary particle diameters of 36 to 11 nm, respectively.

Fig. 8 shows the average primary particle diameter of the product powders obtained by nitrogen adsorption (BET) [83] as a function of the airflow rate at a production rate of 300 g/h.

The average particle diameter decreases with increasing airflow rate. The increased amount of oxygen along with higher gas velocities leads to enhanced oxygen availability and reactant mixing by turbulence. This reduces the flame height and the fuel/precursor is consumed faster. However, large amounts of inert gas (nitrogen) are delivered to the flame as well, which can significantly lower flame temperature. At lower flame temperatures the particle growth and sintering rates are decreased, thus smaller particles are formed. The

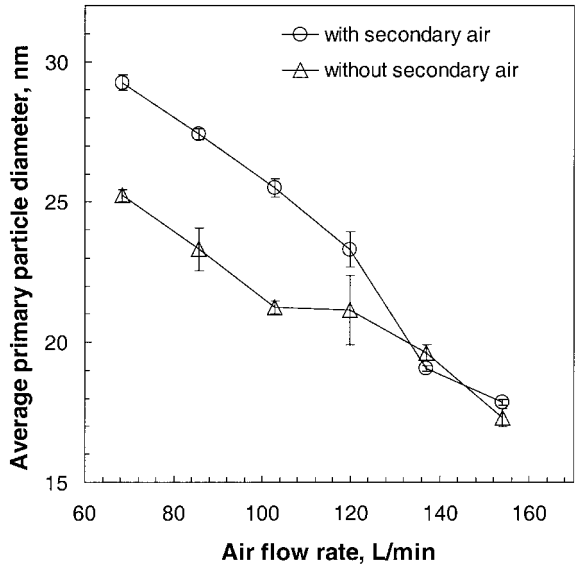

Figure 8. Average primary particle diameter obtained by nitrogen adsorption (BET) as a function of airflow rate with (circles) and without (triangles) secondary air entrainment at production rates of 300 g/h in the reactor of Figure 7.

effect of air entrainment into this flame reactor was investigated by encasing the flame in a stainless steel chimney [17]. In Fig. 8 the average primary particle diameter of the product silica powders in the absence (circles) and in the presence of a chimney surrounding the flame (triangles) are shown. In the absence of the chimney, air from the surroundings can be entrained into the flame leading to enhanced fuel consumption. This leads to higher flame temperatures, which increases the sintering rate and leads to the formation of larger particles for airflow rates less than 120 L/min, Fig. 8. At high airflow rates, however, enough air is provided to diminish the effect of entrained (secondary) air availability. The average primary particle diameter is almost identical with or without the chimney, indicating that at high production rates that are typically encountered in industry, air entrainment is not a crucial parameter affecting product particle characteristics.

By varying the hydrogen flow rate the powder composition can be closely controlled, since the flame temperature is directly affected. At high hydrogen flow rates (36.5 L/min) pure silica powders were obtained, while decreasing the hydrogen flow rate increases the carbon weight fraction of the product powder. However, the specific surface area of these powders made at powder production rates of 300 g/h decreases slightly, when increasing the hydrogen flow rate, due to higher flame temperatures. Keeping the hydrogen and air flow rates constant and increasing the production rate from 125 to 700 g/h, the specific surface area is decreased from 222 to 75 m^2/g. Increasing the production rate, however, increases the hydrocarbon fuel input to the flame by HMDSO, in contrast to the increase of hydrogen, where the hydrocarbon fuel (HMDSO) concentration was constant. This leads to enhanced carbon formation as well as increased flame heights and the carbon content of the powder increases which was determined by thermogravimetric analysis [17]. In this hydrogen/air diffusion flame reactor silica-carbon composite particles were only formed above a molar C/H ratio of 0.12, which was consistent with the onset of soot formation of acetylene-hydrogen mixtures in air diffusion flames observed by Schug et al. [84]. With C/H < 0.12, however, perfectly white silica powders were produced.

3 Nanoparticles by Combustion of Liquid Droplets

In flame spray pyrolysis (FSP), sometimes called liquid flame spray (LFS), the heat is provided by the combustion of a gaseous or liquid fuel and the precursor itself. Multicomponent oxide powders such as beta-$SrMnO_3$ and $NiMn_2O_4$ [85], and superconductors [68,86], alumina [87] as well as $BaTiO_3$ [88] have been made by pyrolysis of solutions containing inorganic precursors in oxy-hydrogen flames. Fully dense primary particles in the size range of 100–500 nm were produced which may have resulted from the rapid disintegration of solution droplets when they enter the high-energy flame [89]. Using organic solvents as liquid fuel, leads to a self-sustaining spray flame. This process has the potential to produce composite mixed-metal oxide powders in the size range of 1 to 200 nm from low cost precursors [90] with production rates up to 250 g/h, as was summarized recently by Laine et al. [19,91]. Typical products synthesized are titania [92] and $MgAl_2O_4$ [93], gamma-Fe_2O_3 [94], alumina [93], manganese oxide, zirconia, and zirconia-ceria [87, 95–97] particles, or very specific functional particles such as beta″-alumina for high temperature solid electrolytes [98,99], to name a few. These processes clearly differ from the conventional spray pyrolysis [100] as the precursor is released from the droplet environment undergoing gas phase reaction and subsequent particle growth by coagulation, surface growth and sintering. Here, direct parallels can be drawn with vapor flame synthesis.

3.1 Flame Spray Reactors

A typical set-up for nanoparticle synthesis by flame spray pyrolysis consists of a unit for the generation and dispersion of droplets, a heat source for initial droplet evaporation and ignition (pilot flame or the spray flame itself for combustible liquids), and an oxidant to facilitate combustion. These parameters control the temperature profile and gas phase reaction of the precursor followed by subsequent particle growth and sintering, taking place within and after the spray flame. The product powder is collected by filtration or thermophoresis. The production of micron-sized liquid droplets can be achieved using various atomizers [101], whereas ultrasonic and gas assist pressurized atomizers are most common in spray combustion. Ultrasonic atomizers show good performance with regard to droplet size and homogeneity [102] and the droplets can be embedded in any gaseous flow for transportation into the reaction zone, where the droplet

velocity can be controlled independently. Gas assist pressurized atomizers, however, are easy to incorporate into the spray flame apparatus and their operation is simple and reliable. High shear rates are needed to disintegrate the liquid jet, thus, high gas velocities are inevitable leading to the high quenching ability of such reactors resulting in small product particles [20].

Fig. 9 shows a turbulent oxygen HMDSO/ethanol spray flame.

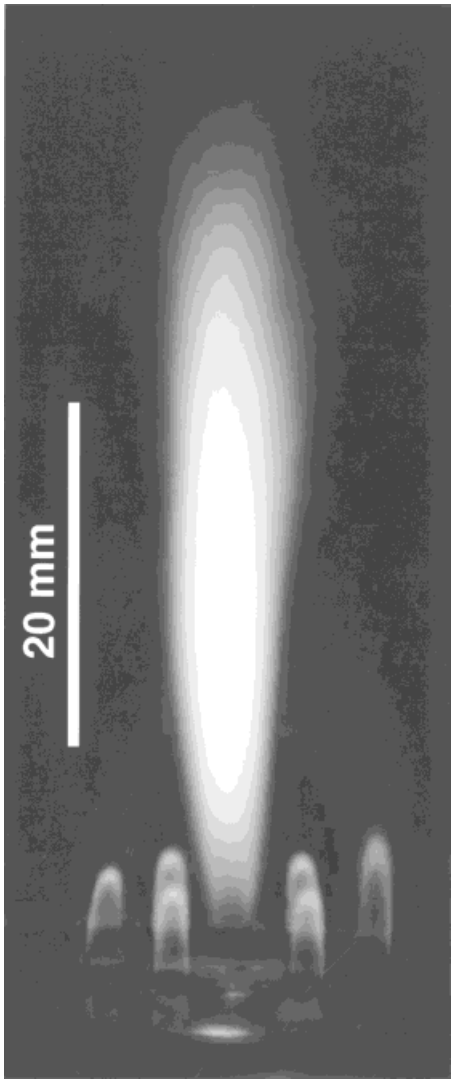

Figure 9. Self-sustaining spray flame, making fumed silica from a 0.1 molar HMDSO in an ethanol solution.

The droplets are formed by a two-phase nozzle where the oxygen acts as both dispersant and oxidant gas disintegrating the liquid jet supplied by a syringe pump. A ring of six premixed methane/oxygen flamelets (shown as little bumps at the base of the spray flame, Fig. 9) provides enough heat for initial droplet evaporation and serves as the ignition source. For a given nozzle opening the droplet size is controlled by the liquid-to-gas mass ratio [101,103]. The product particles are collected on a glass fiber filter. With the current set-up a variety of metal and mixed metal oxide nanoparticles such as SiO_2, TiO_2, Bi_2O_3, Al_2O_3, $BaTiO_3$ all in the size range below 30 nm have been prepared in our laboratories.

3.2 Effect of Spray Composition

3.2.1. Precursor Liquid Composition

The precursor composition is a key parameter in flame spray pyrolysis (FSP) in order to achieve the preferred product properties. The choice of precursor depends on cost, reactivity, selectivity (e.g. suppression of carbide formation during the production of $BaTiO_3$), stability before processing, and low toxicity. In wet chemical processing of metal oxides and mixed metal oxides, nitrate precursors are often used. Spraying these precursors as aqueous solutions into hot wall reactors resulted in micrograined amorphous powders as demonstrated by Jokanovic et al. [104]. However Karthikeyan et al. [95] found that when a solution of nitrate precursors and organic solvents (e.g. ethanol, iso-propanol) was sprayed into a pilot flame crystalline and dense alumina nanoparticles were made. In our laboratories we produced bismuth oxide from bismuth nitrate in an ethanol solution that was stabilized with 15% nitric acid. These particles find applications in pharmaceuticals [105] and varistors [106]. Crystalline nanoparticles with an average primary particle diameter down to 13 nm were obtained as determined by nitrogen adsorption (BET) and X-ray diffraction (XRD). Fig. 10 shows a TEM micrograph of crystalline Bi_2O_3 particles prepared by flame spray pyrolysis with a BET average primary particle diameter of 27 nm.

The flame was self-sustaining, even though a nitrate precursor was used.

Vollath et al. [107], and Karthikeyan et al. [95] reported that organometallic precursors form particles of improved homogeneity and with smaller grain size distributions when compared to aqueous solutions. This was attributed to the

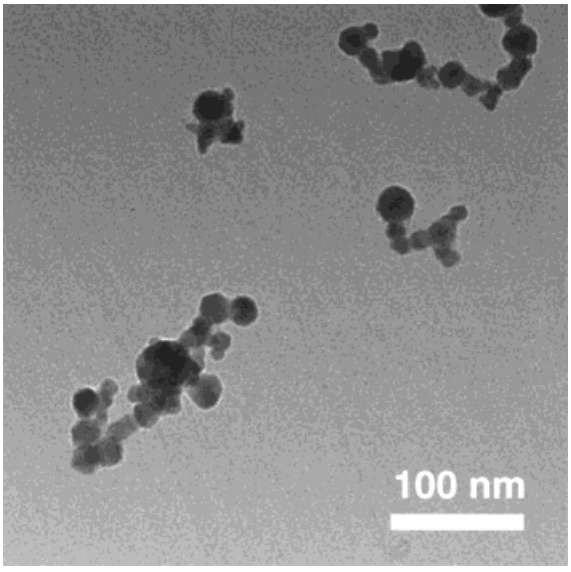

Figure 10. Transmission electron micrograph of Bi_2O_3 particles made directly by flame spray pyrolysis (FSP).

presence of water droplets or vapor in the reaction zone producing larger particles and was also observed for higher gas flow rates during production of Bi_2O_3 in our laboratories. Even though organometallic precursors are typically more expensive than their halide or nitrate counterparts, the higher product powder quality (better homogeneity and smaller grain size distribution) may compensate for this. Organometallic precursors are often used in combination with an organic solvent (e.g. alkoxides, acetates, acetylacetonates, etc.), resulting in a self-sustaining spray flame.

An elegant way for manufacture of mixed metal precursors was performed by the implementation of the stoichiometric preset of the desired metals into an organic complex [90]. This concept was successfully applied in production of mullite nanoparticles [91] from alkoxide complexes. In another example, $BaTiO_3$ was synthesized from organometallic precursors, where the precursor preparation from ethanol, TTIP and barium-II-ethyl-hexanoate first formed a Ba-Ti alkoxide [108], which was then introduced into our self-sustaining spray flame reactor. $BaTiO_3$ nanoparticles with an average particle size less than 50 nm were produced, which are smaller than those of Brewster and Kodas [88] who made them by spraying nitrate solutions in oxy-hydrogen flames. The precursor release from the droplet, its decomposition and gas phase reaction are important steps in formation of the final product. The precursor composition plays an important role, but this is still not well understood. For example, it was found by Gardner and Messing [109] that 14 nm MgO nanoparticles were formed from $Mg(CH_3COO)_2$, but not from $Mg(NO_3)_2$. Although both salts yielded particles consisting of nanocrystallites, it was proposed that the oxidation of the carbonaceous residue from the acetate resulted in non-agglomerated nanocrystallites. In order to improve phase homogeneity, gelation of the precursor within the fuel droplet could be advantageous.

3.2.2. Liquid Fuel Composition

Besides the precursor composition, Mädler et al. [20] found that the total energy content of the spray flame and the evaporation rate of the liquid fuel are important parameters controlling the product powder properties. Fig. 11 shows the specific surface area of the SiO_2 powder product as a function of the dispersion gas flow rate in a self-sustaining spray flame, using a 0.1 molar mixture of HMDSO and ethanol (diamonds) and iso-octane (circles) as fuel, respectively.

Increasing the dispersion gas (oxygen) flow rate, the specific surface area increases from 220 m^2/g (at 1.7 L/min) to a maximum value of 320 m^2/g (at 3 L/min) and then drops to 230 m^2/g (at 4.4 L/min) for higher flow rates using ethanol as solvent. At low oxidant flow rates the specific surface area increases with increasing oxidant flow rate as the height of the spray flame is reduced, leading to shorter residence times, thus, reducing the time for particle growth. At high oxidant flow rates, the fuel is consumed faster leading to shorter flames (Fig. 9) and higher maximum temperature. The fuel

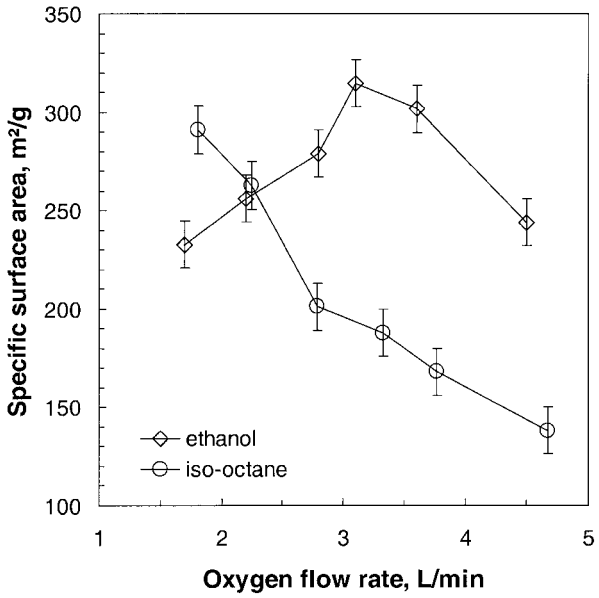

Figure 11. Specific surface area of SiO_2 particles made by FSP for 0.1 molar HMDSO/organic fuel solution as a function of dispersion gas (oxygen) flow rate using ethanol (diamonds) and iso-octane (circles) as solvent.

and precursor reaction is more intense for high oxygen flow rates, and takes place in a smaller unit volume initiating fast precursor release at higher temperatures, thus, leading to enhanced sintering rates and, therefore, to smaller specific surface areas. With iso-octane as fuel, only the declining branch of the specific surface area is found (Fig. 11), has a 1.5 times higher enthalpy content and a 1.5 times higher evaporation rate during the combustion compared to ethanol [110]. Since the temperature of the flame is substantially higher for iso-octane, the specific surface area is substantially lower (120 m^2/g at 4.6 L/min) for higher flow rates, even though the SiO_2 production rate is 2.1 times that of the HMDSO/ethanol mixture for fixed molar ratios of HMDSO to solvent. Here, the liquid fuel composition is an important temperature profile defining parameter and therefore influences particle growth and sintering. A similar trend was found by Briesen et al. [35] who reported a drastic drop in the specific surface area of silica at higher adiabatic flame temperatures which is in accordance with the present data for the energy of the spray flames comparing ethanol and iso-octane fuels. This example clearly shows the importance of controlling the droplet evaporation and combustion in production of oxide particles by flame spray pyrolysis. Information on burning rates and droplet lifetime and thus precursor decomposition (reaction) can be gained from spray combustion models and incorporated in existing models of particle synthesis in vapor flames.

4 Modeling of Nanoparticle Formation and Growth

The development of mathematical models for simulation of particle formation and growth is intriguing because they connect input parameters such as reactant state, composition,

and volume flow as well as reactor geometry, to particle or powder characteristics such as particle size, agglomerate structure, porosity, morphology, and crystallinity. This information can contribute to process optimization and control of existing and new products, accelerate scale-up, minimize down-time due to modifications and increase yield of the process, thus decreasing the cost of raw materials per product.

In the literature, there are numerous models (modisperse-, moment-, sectional-, and Monte-Carlo-types) describing particle growth in flames. An introduction to particle dynamics models is given e.g. by Kodas and Hampden-Smith [25], in which they discuss the advantages and disadvantageous of certain approaches. The latest advances in the calculation of sintering rates for oxide nanoparticles was achieved by accounting for the dependence of the melting point on particle size for titania and alumina [111] and for silica [112]. Experimental data on particle size evolution as obtained by thermophoretic sampling and information about the flame temperature from FTIR at the same location [4] can be used to develop models that describe the evolution of particle growth [5]. From this data, the effective rates of reaction on the particle surface can be extracted.

One result of a better understanding of the effect of detailed flow fields and detailed temperature information on particle growth could be design of special burners. A first attempt was used to visualize flow patterns and gas concentration evolution of different diffusion burner geometries [8], putting emphasis on the mixing of the concentric jets. The mixing is controlled by the velocity gradient of co-flowing jets. The velocity vectors of the jet and lines of constant argon molar fraction, which indicate the precursor stream, are calculated by computational fluid dynamics and are presented in Fig. 12.

Increasing the oxygen flow from 1.5 to 8 L/min in the third (outer) tube and keeping the other flow rates constant significantly increases mixing and forms a toroidal recirculating vortex in the central region. The local precursor concentration indicated by argon diminishes almost instantaneously for the high oxygen flow rate (8 L/min), thus the mixing and dilution of reactants occurs close to the burner mouth. Silica particles formed under these conditions are highly agglomerated consisting of small primary particles, Fig. 12b. This particle shape typically occurs for low residence times of the particles in the hot flame zone as well as for low flame temperatures. However, for a low oxygen flow rate (1.5 L/min) the residence time of the particles is much longer and cooling by mixing with cold gases is less pronounced. During formation of these particles the time for sintering is long enough to form larger spherical silica particles, Fig. 12a.

Chao and Axelbaum [113] recently introduced an analytical solution for a diffusion flame formed from three concentric tubes similar to that calculated with CFD. They extended the Burke-Schumann methodology [114] and included a third stream. The ability to have analytical solutions for special cases of a diffusion flame consisting of three reactant streams may tempt the testing of the performance and further improve computational fluid dynamic software. Particle growth models can be implemented as demonstrated by Schild et al. [115] and Pyykönen and Jokiniemi [116] for TiO_2 formation in a turbular flow reactor, and aerosol formation in a laminar flow reactor, respectively. These techniques provide a very effective tool for the simulation of particle formation processes in complex reactor geometries under real production conditions. The formation of alumina from aluminium-sec-butoxide was studied experimentally by Johannessen et al. [6], and was compared with a commercially available computational fluid dynamics (CFD-) package to simulate gas temperatures and velocity profiles of burners. After the temperature and gas composition fields were calculated, the monodisperse particle growth model by Kruis et al. [117] was implemented, which was modified with a dilution factor [118] obtained from the CFD calculations. Following characteristic trajectory lines, the model gives a good prediction of the specific surface area of the product particles. This model was extended [7] to the formation of titania particles and was validated by comparison with experiments conducted in a single (classic) or double (inverted) diffusion methane/air flame reactor producing TiO_2 particles [31]. Besides the final average product particle size, the degree of aggregation

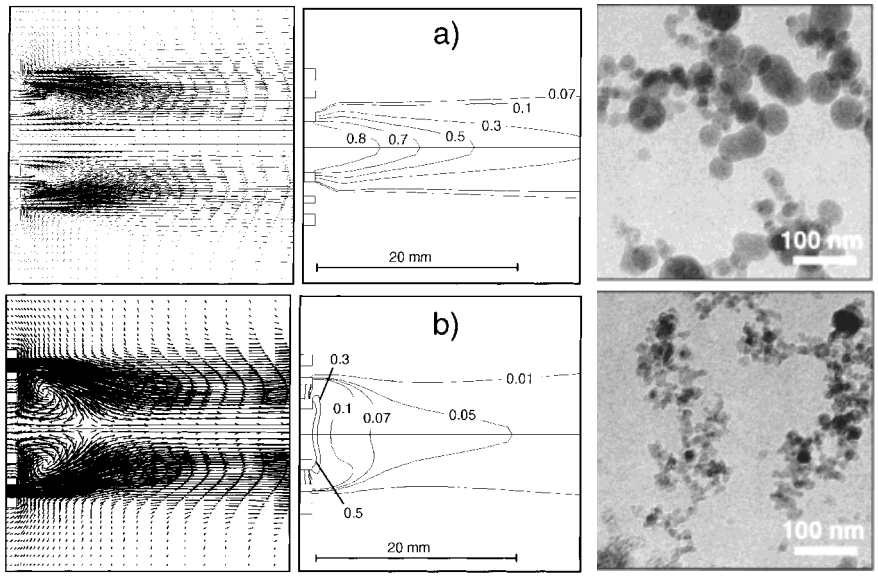

Figure 12. Velocity vectors (right), iso-molar lines of argon fraction (middle), both calculated by computational fluid dynamics, and TEM micrographs of SiO_2 product powder (right), obtained from a micro scale diffusion flame reactor [8]. The flow rate of oxygen through the third (outer) tube is 1.5 L/min (a) and 8 L/min (b), while the flow rates of argon (center tube) and methane (second tube) were kept constant 0.25 and 0.4 L/min, respectively (courtesy of K. Wegner, ETHZ).

(number of primary particles per agglomerate) was predicted very well when compared to the data obtained with small angle X-ray scattering [32].

In flame spray pyrolysis, spray combustion models provide information on burning rates and droplet lifetime and thus precursor decomposition and reaction, which can be combined with models for aerosol growth. Droplet evaporation, ignition, and combustion have to be taken into consideration in making assumptions in order to simplify the model [119]. Several approximations have to be considered and validated, including: drop breakup, turbulent droplet dispersion, effects on the enveloping flame, and effects of drop dynamics and turbulence on drop transport rates [120]. Furthermore, the spray properties involved, have to be critically reviewed in order to implement or exclude basic phenomena in the model such as: droplet slip and internal circulation, transient heating of the droplets, multicomponent fuel vaporization and combustion and vaporization of droplet arrays, and groups [121].

Further implementation of more sophisticated models of droplet evaporation and burning [122], accounting for multicomponent mixtures [123] and combustion modes (e.g. single droplet, group, or sheath combustion) [124–127] developed for spray combustion in turbine and automotive engineering, will add fundamental understanding to the flame spray pyrolysis processes accounting for the transport and chemistry of burning sprays [128].

Besides the implementation of numerical codes describing centerline time dependent droplet history, accounting for multicomponent mixtures, the flow field of the spray flame, the droplet combustion, and the temperature profile can be modeled by applying computational fluid dynamics. As for aerosol reactors [115,129], solvers, using a finite volume technique, can be used to describe the flow field and the droplet combustion of spray flames by solving systems of differential equations. Then, the effect of the released heat of reaction on the temperature distribution in the flame and the density of the gases can be considered in the fluid dynamics model.

After the release of the precursor from the droplet environment and its reaction, the subsequent growth of particles from molecules occurs by surface growth and/or coagulation and sintering leading to a steadily growing particle size. The description for the rate change of the number concentration of particles is based on detailed sectional models [130]. Although there are a number of solutions to the population balance equation depending on approximations on the shape of the size distribution, a simple sectional technique can be used [131]:

$$\frac{dN_i}{dt} = \{N_{i-1}\sum_{j=1}^{i-2} 2^{j-i+1}\beta_{i-1,j}N_j + \frac{1}{2}\beta_{i-1,i-1}N_{i-1}^2 - N_i\sum_{j=1}^{i-1} 2^{j-1}\beta_{i,j}N_j - N_i\sum_{j=1}^{M}\beta_{i,j}N_j\}\rho_g \quad (1)$$

The first term on the right hand side (RHS) of the equation refers to the rate of birth of agglomerates in section i by collision between agglomerates of the i-1 section and j sections ranging from 1 to i-2, where N is the number concentration, β is the collision frequency function and ρ_g the density of the gas. The second RHS term refers to the birth of agglomerates in the i^{th} section by the collision of agglomerates of equal size (i-1). The third RHS term accounts for the death rate of agglomerates in section i by collisions between these agglomerates and smaller ones. The fourth RHS term corresponds to the death rate of agglomerates in section i by collisions between these agglomerates and agglomerates in the same or higher size intervals. Furthermore, the effect of sintering on the agglomerate surface area a_i is [132]:

$$\frac{da_i}{dt} = -\frac{1}{\tau_{s,i}}(a_i - a_{s,i}) \quad (2)$$

where $\tau_{s,i}$ is the characteristic sintering time (the time needed to reduce the excess surface area of an agglomerate over that of an equal mass sphere by approximately 63 %) and $a_{s,i}$ is the surface area of a completely fused (spherical) agglomerate. The inclusion of theoretical and background knowledge of particle formation in computational tools for spray flame pyrolysis may lead to revolutionary improvements in the understanding of the formation process of these particles and optimal design of flame spray combustion, thus opening up a new area for designing particles with closely controlled characteristics.

5 Concluding Remarks

The formation and control of particle characteristics in flame aerosol reactors from gaseous and liquid precursors was reviewed. Reactant mixing, additives, and external electric fields are effective tools for controlling powder product characteristics. A relationship between laboratory-scale experiments and conditions close to those used in industrial pilot-scale units is developed with a systematic study of silica-carbon composite production at concentrations up to 10 % solid fraction by mass. Flame spray pyrolysis further broadens the spectrum of flame made powders and their various applications as there are more liquid than gaseous precursors for particle synthesis. Even particles with pre-defined stoichiometric composition can be easily produced. It has been shown that key parameters for vapor flame processes are also important for flame spray pyrolysis and that the liquid fuel and precursor composition provides additional variation for special particle design and control.

Fundamental studies on particle growth, simultaneously measuring flame temperature and particle size evolution by thermophoretic sampling in the flame can be used to develop models describing the particle growth without adjusting parameters and thus revealing the dominant physicochemical phenomena. The combination of computational fluid dynamics along with further development of particle growth models helps to rank aerosol reactor designs and to guide

the operation of large-scale facilities for production of particles with well-defined characteristics.

Acknowledgements

We would like to acknowledge the financial support of the Swiss National Science Foundation SNF 2100-055469.98, and also the assistance of Osama I. Arabi-Katbi (University of Cincinnati, Cincinnati, OH, U.S.A. and currently at Degussa-Hüls, Theodore, AL, U.S.A.) with the FTIR/thermophoretic sampling.

Received: February 19, 2001 [CET 1375]

References

[1] Mezey, E. J., Pigments and Reinforcing Agents, in: *Vapor Deposition* (C. F. Palmer, J. H. Oxley, J. M. Blocher Jr., Eds.) John Wiley and Sons, New York 1966, pp. 423–449.
[2] Pratsinis, S. E., *Prog. Energy Combust. Sci. 24* (1998) No. 3, pp. 197–219.
[3] Morrison Jr., P. W., Raghavan, R., Timpone, A. J., Artelt, C. P., Pratsinis, S. E., *Chem. Mater. 9* (1997) No. 12, pp. 2702–2708.
[4] Arabi-Katbi, O. I., Pratsinis, S. E., Morrison Jr., P. W., Megaridis, C. M., *Combust. Flame 124* (2001) No. 4, pp. 560–572.
[5] Pratsinis, S. E., Arabi-Katbi, O. I., Megaridis, C. M., Morrison Jr., P. W., Tsantilis, S., Kammler, H. K., *J. Metastable Nanocrystalline Mater. 8* (2000) pp. 511–518.
[6] Johannessen, T., Pratsinis, S. E., Livbjerg, H., *Chem. Eng. Sci. 55* (2000) No. 1, pp. 177–191.
[7] Johannessen, T., Pratsinis, S. E., Livbjerg, H., *Powder Technol*. (2001) in press.
[8] Wegner, K., Pratsinis, S. E., Aerosol-based Flame Synthesis: A micro-reactor for Silica Nanoparticles, in: *Innovative Processing of Films and Nanocrystalline Powders* (K. L. Choy, Editor) Imperial College Press, London 2001, in press.
[9] Katz, J. L., Miquel, P. F., *NanoStructured Mater. 4* (1994) No. 5, pp. 551–575.
[10] Vemury, S., Pratsinis, S. E., *J. Am. Ceram. Soc. 78* (1995) No. 11, pp. 2984–2992.
[11] Zachariah, M. R., Aquino, M. I., Shull, R. D., Steel, E. B., *NanoStructured Mater. 5* (1995) No. 4, pp. 383–392.
[12] Byers, J. T., McNeish, A. A., Current Advances in Tire Compounding Technology for Low Rolling Resistance, Carbon Black World Conference 1997, San Antonio, TX, March 19–21.
[13] Briesen, H., Fuhrmann, A., Pratsinis, S. E., Electrically Assisted Aerosol Reactors Using Ring Electrodes, in: *Nanostructured Powders and Their Industrial Applications* (G. Beaucage, J. E. Mark, G. T. Burns, D.-W. Hua, Eds.) Materials Research Society, San Francisco, CA 1998, pp. 3–14.
[14] Kammler, H. K., Pratsinis, S. E., *Chem. Eng. Process. 39* (2000) No. 3, pp. 219–227.
[15] Spicer, P. T., Artelt, C., Sanders, S., Pratsinis, S. E., *J. Aerosol Sci. 29* (1998) No. 5/6, pp. 647–659.
[16] Kammler, H. K., Pratsinis, S. E., *J. Nanoparticle Res. 1* (1999) No. 4, pp. 467–477.
[17] Kammler, H. K., Mueller, R., Senn, O., Pratsinis, S. E., *AIChE J.* (2001) in press.
[18] Stark, W. J., Wegner, K., Pratsinis, S. E., Baiker, A., *J. Catal. 197* (2001) No. 1, pp. 182–191.
[19] Laine, R. M., Baranwal, R., Hinklin, T., Treadwell, D., Sutorik, A., Bickmore, C., Waldner, K., Neo, S. S., *Key. Eng. Mat. 159* (1999) No. 1, pp. 17–24.
[20] Mädler, L., Kammler, H. K., Mueller, R., Pratsinis, S. E. (2001) unpublished work.
[21] Ulrich, G. D., *Chem. Eng. News 62* (1984) No. 32, pp. 22–29.
[22] Granqvist, C. G., Buhrman, R. A., *J. Appl. Phys. 47* (1976) No. 5, pp. 2200–2219.
[23] Gurav, G., Kodas, T., Pluym, T., Xiong, Y., *Aerosol Sci. Technol. 19* (1993) No. 4, pp. 411–452.
[24] Wooldridge, M. S., *Prog. Energy Combust. Sci. 24* (1998) No. 1, pp. 63–87.
[25] Kodas, T. T., Hampden-Smith, M. J., *Aerosol Processing of Materials*, Wiley-VCH, New York 1999.
[26] Braun, J. H., *J. Coat. Technol. 69* (1997) No. 868, pp. 59–72.
[27] Braun, J. H., Baidins, A., Marganski, R. E., *Prog. Org. Coat. 20* (1992) No. 2, pp. 105–138.
[28] Hartmann, W., Liu, A. T., Peuckert, D., Kleinschmit, P., *Mater. Sci. Eng. A109* (1989) pp. 243–246.
[29] Sniegowski, J. J., de Boer, M. P., *Annu. Rev. Mater. Sci. 30* (2000) pp. 299–333.
[30] Donnet, J., Bansal, R. C., Wang, M. J., *Carbon Black*, Marcel Decker, New York 1993.
[31] Pratsinis, S. E., Zhu, W., Vemury, S., *Powder Technol. 86* (1996) No. 1, pp. 87–93.
[32] Hyeon-Lee, J., Beaucage, G., Pratsinis, S. E., Vemury, S., *Langmuir 14* (1998) No. 20, pp. 5751–5756.
[33] Zhu, W., Pratsinis, S. E., *AIChE J. 43* (1997) No. 11A, pp. 2657–2664.
[34] Zhu, W., Pratsinis, S. E., Flame Synthesis of Nanosize Powders: Effect of Flame Configuration and Oxidant Composition, in: *Nanotechnology* (G.-M. Chow, K. E. Gonsalves, Eds.) American Chemical Society, Washington 1996, pp. 64–78.
[35] Briesen, H., Fuhrmann, A., Pratsinis, S. E., *Chem. Eng. Sci. 53* (1998) No. 24, pp. 4105–4112.
[36] Zachariah, M. R., Semerjian, H. G., *High Temp. Sci. 28* (1990) pp. 113–125.
[37] Ehrman, S. H., Friedlander, S. K., Zachariah, M. R., *J. Aerosol Sci. 29* (1998) No. 5/6, pp. 687–706.
[38] Formenti, M., Juillet, F., Meriaudeau, P., Teichner, S. J., Vergnon, P., *J. Colloid Interface Sci. 32* (1972) No. 1, pp. 79–89.
[39] Ulrich, G. D., Milnes, B. A., Subramanian, N. S., *Combust. Sci. Technol. 14* (1976) pp. 243–249.
[40] Ulrich, G. D., Riehl, J. W., *J. Colloid Interface Sci. 87* (1982) No. 1, pp. 257–265.
[41] Akhtar, M. K., Pratsinis, S. E., Mastrangelo, S. V. R., *J. Am. Ceram. Soc. 75* (1992) No. 12, pp. 3408–3416.
[42] Akhtar, M. K., Pratsinis, S. E., Mastrangelo, S. V. R., *J. Mater. Res. 9* (1994) No. 5, pp. 1241–1249.
[43] Fotou, G. P., Scott, S. J., Pratsinis, S. E., *Combust. Flame 101* (1995) No. 4, pp. 529–538.
[44] Vemury, S., Pratsinis, S. E., *Appl. Phys. Lett. 66* (1995) No. 24, pp. 3275–3277.
[45] Vemury, S., Pratsinis, S. E., *J. Aerosol Sci. 27* (1996) No. 6, pp. 951–966.
[46] Vemury, S., Pratsinis, S. E., Kibbey, L., *J. Mater. Res. 12* (1997) No. 4, pp. 1031–1042.
[47] Katzer, M., Ph. D. Thesis, Universität Karlsruhe (TH) 2000.
[48] Eckbreth, A. C., *Laser Diagnostics for Combustion, Temperature and Species*, Abacus Press, Kent, UK, 1988.
[49] Zachariah, M. R., Shull, R. D., McMillin, B. K., Biswas, P., In-situ Characterization and Modeling of the Vapor-phase Formation of a Magnetic Nanocomposite, in: *Nanotechnology* (G.-M. Chow, K. E. Gonsalves, Eds.) American Chemical Society, Washington 1996, pp. 42–63.
[50] Glumac, N. G., Chen, Y.-J., *J. Mater. Res. 13* (1998) No. 9, pp. 2572–2579.
[51] McMillin, B. K., Biswas, P., Zachariah, M. R., *J. Mater. Res. 11* (1996) No. 6, pp. 1552–1561.
[52] Colibaba-Evulet, A., Singhal, A., Glumac, N., *Combust. Sci. Technol. 157* (2000) pp. 129–139.
[53] Best, P. E., Chien, P. L., Carangelo, R. M., Solomon, P. R., Danchak, M., Ilovivi, I., *Combust. Flame 85* (1991) No. 3/4, pp. 309–318.
[54] Solomon, P. R., Best, P. E., Fourier Transform Infrared Emission/Transmission Spectroscopy in Flames, in: *Combustion Measurements* (N. Chigier, Editor) Hemishpere Publication Corp., New York 1991, pp. 385–444.
[55] Farquharson, S., Charpenay, S., DiTaranto, M. B., Rosenthal, P. A., Zhu, W., Pratsinis, S. E., In-situ Particle Size and Shape Analysis During Flame Synthesis of Nanosize Powders, in: *Synthesis and Characterization of Advanced Materials* (M. A. Serio, D. M. Gruen, R. Malhotra, Eds.) American Chemical Society, Orlando, FL 1998, pp. 170–186.
[56] Best, P. E., Carangelo, R. M., Markham, J. R., Solomon, P. R., *Combust. Flame 66* (1986) No. 1, pp. 47–66.
[57] Santoro, R. J., Yeh, T. T., Horvath, J. J., Semerjian, H. G., *Combust. Sci. Technol. 53* (1987) No. 2/3, pp. 89–115.
[58] Boedecker, L. R., Dobbs, G. M., *Combust. Sci. Technol. 46* (1986) pp. 301–323.
[59] Glassman, I., *Combustion,* Academic Press, San Diego 1996.
[60] Megaridis, C. M., Ph. D. Thesis, Brown University 1987.
[61] Dobbins, R. A., Megaridis, C. M., *Langmuir 3* (1987) No. 2, pp. 254–259.

[62] Lindackers, D., Janzen, C., Rellinghaus, B., Wassermann, E. F., Roth, P., *NanoStructured Mater. 10* (1998) No. 8, pp. 1247–1270.
[63] Lindackers, D., Strecker, M. G. D., Roth, P., Janzen, C., Pratsinis, S. E., *Combust. Sci. Technol. 123* (1997) pp. 287–315.
[64] Lindackers, D., Strecker, M. G. D., Roth, P., *NanoStructured Mater. 4* (1994) No. 5, pp. 545–550.
[65] Roth, P., Hospital, A., *J. Aerosol Sci. 25* (1994) No. 1, pp. 61–73.
[66] Janzen, C., Stecker, M. G. D., Roth, P., *KONA Powder Part. 17* (1999) pp. 114–121.
[67] Kee, R. J., Grcar, J. F., Smooke, M. D., Miller, J. A., *PREMIX. A Fortran Program for Modeling Steady Laminar One-dimensional Premixed Flames.* 1985, Sandia National Laboratories: Livermore. pp. 85–8240.
[68] Zachariah, M. R., Huzarewicz, S., J. Mater. Res. 6 (1991) No. 2, pp. 264–269.
[69] Hung, C.-H., Katz, J. L., *J. Mater. Res. 7* (1992) No. 7, pp. 1861–1869.
[70] Hung, C.-H., Miquel, F., Katz, J. L., *J. Mater. Res. 7* (1992) No. 7, pp. 1870–1875.
[71] Miquel, P. F., Hung, C. H., Katz, J. L., *J. Mater. Res. 8* (1993) No. 9, pp. 2404–2413.
[72] Miquel, P. F., Katz, J. L., *J. Mater. Res. 9* (1994) No. 3, pp. 746–754.
[73] Ehrman, S. H., Friedlander, S. K., Zachariah, M. R., *J. Mater. Res. 14* (1999) No. 12, pp. 4551–4561.
[74] Bond, G. C., Tahir, S. F., *Appl. Catal. 71* (1991) No. 1, pp. 1–31.
[75] Bosch, H., Janssen, F., *Catal. Today 2* (1988) No. 4, pp. 369–532.
[76] Engweiler, J., Baiker, A., Appl. Catal. A-Gen. 120 (1994) No. 1, pp. 187–205.
[77] Reiche, M. A., Hug, P., Baiker, A., *J. Catal. 192* (2000) No. 2, pp. 400–411.
[78] U.S. Pat. 4789533 (1988) Lonza Ldt. (Inv.: Baiker, A., Dollenmeier, P., Glinski, M.).
[79] Wang, M.-J., Mahmud, K., Murphy, L. J., Patterson, W. J., *Kautsch. Gummi Kunstst. 51* (1998) No. 5, pp. 348–360.
[80] Padula, S., Tire Fuel Economy Labeling – An Update, Tire Industry Conference 1995, Hilton Head, SC, March 9–10.
[81] Blume, H., *Kautsch. Gummi Kunstst. 53* (2000) No. 6, pp. 338–345.
[82] Pat. DE 830 786 (1952) Degussa (Inv.: Kloepfer, H.).
[83] Brunauer, S., Emmett, P. H., Teller, E., *J. Am. Chem. Soc. 60* (1938) pp. 309–319.
[84] Schug, K. P., Manheimer-Timnat, Y., Yaccarino, P., Glassman, I., *Combust. Sci. Technol. 22* (1980) pp. 235–250.
[85] Kriegel, R., Töpfer, J., Preuss, N., Grimm, S., Böer, J., *J. Mater. Sci. Lett. 13* (1994) No. 15, pp. 1111–1113.
[86] U.S. Pat. 5 814 585 (1998) Merck Patent GmbH (Inv.: Feldmann-Schlobohm, G., Mueller, B., Kuntz, M., Raulin, D., Riddle, R.).
[87] Tikkanen, J., Gross, K. A., Berndt, C. C., Pitkanen, V., Keskinen, J., Raghu, S., Rajala, M., Karthikeyan, J., *Surf. Coat. Technol. 90* (1997) No. 3, pp. 210–216.
[88] Brewster, J. H., Kodas, T. T., *AIChE J. 43* (1997) No. 11, pp. 2665–2669.
[89] Law, C. K., *Prog. Energy Combust. Sci. 8* (1982) pp. 171–201.
[90] Narayanan, R., Laine, R. M., *App. Organomet. Chem. 11* (1997) No. 10–11, pp. 919–927.
[91] Laine, R. M., Hinklin, T., Williams, G., Rand, S. C., *J. Metastable Nanocrystalline Mater. 8* (2000) pp. 500–510.
[92] Bickmore, C. R., Waldner, K. F., Baranwal, R., Hinklin, T., Treadwell, D. R., Laine, R. M., *J. Eur. Ceram. Soc. 18* (1998) No. 4, pp. 287–297.
[93] Bickmore, C. R., Waldner, K. F., Treadwell, D. R., Laine, R. M., *J. Am. Ceram. Soc. 79* (1996) No. 5, pp. 1419–1423.
[94] Grimm, S., Schultz, M., Barth, S., Muller, R., *J. Mater. Sci. 32* (1997) No. 4, pp. 1083–1092.
[95] Karthikeyan, J., Berndt, C. C., Tikkanen, J., Wang, J. Y., King, A. H., Herman, H., *NanoStructured Mater. 8* (1997) No. 1, pp. 61–74.
[96] Sokolowski, M., Sokolowska, A., Michalski, A., Gokieli, B., *J. Aerosol Sci. 8* (1977) pp. 219–229.
[97] Tani, T., Takatori, K., Watanabe, N., Kamiya, N., *J. Mater. Res. 13* (1998) No. 5, pp. 1099–1102.
[98] Sutorik, A. C., Neo, S. S., Treadwell, D. R., Laine, R. M., *J. Am. Ceram. Soc. 81* (1998) No. 6, pp. 1477–1486.
[99] Treadwell, D. R., Sutorik, A. C., Neo, S. S., Laine, R. M., Svedberg, R. C., Synthesis of Beta″-Alumina Polymer Precursor and Ultrafine Beta″-Alumina Composition Powders, in: *Synthesis and Characterization of Advanced Materials* (M. A. Serio, D. M. Gruen, R. Malhotra, Eds.) American Chemical Soc., Washington 1998, pp. 146–156.
[100] Messing, G. L., Zhang, S. C., Jayanthi, G. V., *J. Am. Ceram. Soc. 76* (1993) No. 11, pp. 2707–2726.
[101] Lefebvre, A. H., *Atomization Spray*, Taylor and Francis, London 1989.
[102] Rodes, C., Smith, T., Crouse, R., Ramachandran, G., *Aerosol Sci. Technol. 13* (1990) No. 2, pp. 220–229.
[103] Perry, R. H., *Perry's Chemical Engineers' Handbook*, McGraw-Hill, New York 1997.
[104] Jokanovic, V., Janackovic, D., Spasic, A. M., Uskokovic, D., *Materials Transactions, JIM 37* (1996) No. 4, pp. 627–635.
[105] Dresow, B., Fischer, R., Gabbe, E. E., Wendel, J., Heinrich, H. C., *Scand. J. Gastroenterol. 27* (1992) No. 4, pp. 333–336.
[106] Metz, R., Delalu, H., Vignalou, J. R., Achard, N., Elkhatib, M., *Mater. Chem. Phys. 63* (2000) No. 2, pp. 157–162.
[107] Vollath, D., Sickafus, K. E., *NanoStructured Mater. 1* (1992) pp. 427–437.
[108] Thomas, R., Dube, D. C., Kamalasanan, M. N., Chandra, S., Bhalla, A. S., *J. Appl. Phys. 82* (1997) No. 9, pp. 4484–4488.
[109] Gardner, T. J., Messing, G. L., *Am. Ceram. Soc. Bull. 63* (1984) No. 12, pp. 1498–1501.
[110] Gutheil, E., *Modellierung technischer Sprayflammen*, VDI Verlag, Düsseldorf 1998.
[111] Xing, Y., Rosner, D. E., *J. Nanoparticle Res. 1* (1999) No. 2, pp. 277–291.
[112] Tsantilis, S., Briesen, H., Pratsinis, S. E., *Aerosol Sci. Technol. 34* (2001) No. 3, pp. 237–246.
[113] Chao, B. H., Axelbaum, R. L., *Combust. Sci. Technol. 156* (2000) pp. 291–314.
[114] Burke, S. P., Schumann, T. E. W., *Ind. Eng. Chem. 20* (1928) No. 10, pp. 998–1004.
[115] Schild, A., Gutsch, A., Muehlenweg, H., Pratsinis, S. E., *J. Nanoparticle Res. 1* (1999) No. 2, pp. 305–315.
[116] Pyykönen, J., Jokiniemi, J., *J. Aerosol Sci. 31* (2000) No. 5, pp. 531–550.
[117] Kruis, F. E., Kusters, K. A., Pratsinis, S. E., Scarlett, B., *Aerosol Sci. Technol. 19* (1993) No. 4, pp. 514–526.
[118] Johannessen, T., Ph. D. Thesis, Technical University of Denmark 1999.
[119] Faeth, G. M., *Prog. Energy Combust. Sci. 3* (1977) pp. 191–224.
[120] Faeth, G. M., *Prog. Energy Combust. Sci. 9* (1983) No. 1–2, pp. 1–76.
[121] Sirignano, W. A., *Prog. Energy Combust. Sci. 9* (1983) No. 4, pp. 291–322.
[122] Abramzon, B., Sirignano, W. A., *Int. J. Heat Mass Transf. 32* (1989) No. 9, pp. 1605–1618.
[123] Hallett, W. L. H., *Combust. Flame 121* (2000) No. 1–2, pp. 334–344.
[124] Chiu, H. H., Liu, T. M., *Combust. Sci. Technol. 17* (1977) pp. 127–142.
[125] Akamatsu, F., Mizutani, Y., Katsuki, M., Tsushima, S., Cho, Y. D., Nakabe, K., *Atom. Sprays 7* (1997) No. 2, pp. 199–218.
[126] Chen, G., Gomez, A., *Combust. Flame 110* (1997) No. 3, pp. 392–404.
[127] Labowski, M., Rosner, D. E., Group Combustion of Droplets in Fuel Clouds, I. Quasi-steady Predictions, in: *Evaporation-Combustion of Fuels* (J. T. Zung, Editor) American Chemical Society, Washington 1978, pp. 63–79.
[128] Gutheil, E., Sirignano, W. A., *Combust. Flame 113* (1998) No. 1–2, pp. 92–105.
[129] Tsantilis, S., Pratsinis, S. E., Haas, V., *J. Aerosol Sci. 30* (1999) No. 6, pp. 785–803.
[130] Landgrebe, J. D., Pratsinis, S. E., *Ind. Eng. Chem. Res. 28* (1989) No. 10, pp. 1474–1481.
[131] Tsantilis, S., Pratsinis, S. E., *AIChE J. 46* (2000) No. 2, pp. 407–415.
[132] Koch, W., Friedlander, S. K., *J. Colloid Interface Sci. 140* (1990) No. 2, pp. 419–427.

